Anomalous spin-lattice relaxation in InP:Fe^{3+} and BaFBr:Eu^{2+} examined with optical detection of electron paramagnetic resonance

1993 J. Phys.: Condens. Matter 5 733

(http://iopscience.iop.org/0953-8984/5/6/010)

J. Phys.: Condens. Matter 5 (1993) 733–746. Printed in the UK

Anomalous spin–lattice relaxation in InP:Fe^{3+} and BaFBr:Eu^{2+} examined with optical detection of electron paramagnetic resonance

F K Koschnick†, M Rac†, J-M Spaeth† and R S Eachus‡

† University of Paderborn, Fachbereich Physik, Warburger Strasse 100, 4790 Paderborn, Federal Republic of Germany

‡ Research Laboratories, Eastman Kodak Company, Rochester, NY 14650-2021, USA

Received 13 August 1992, in final form 10 November 1992

Abstract. The Eu^{2+} defect in BaFBr and the Fe^{3+} defect in InP were investigated by optical detection of electron paramagnetic resonance (ODEPR). For both defects allowed ($\Delta m_S = \pm 1$) and forbidden ($\Delta m_S = \pm 2$) ODEPR transitions were observed. Some of the allowed ODEPR transitions showed an anomalous change of sign indicating a spin polarization enhancement. This anomalous behaviour of both spin systems ($S = 7/2$ for Eu^{2+} in BaFBr and $S = 5/2$ for Fe^{3+} in InP) arises from spin–lattice relaxations within the Eu^{2+} and Fe^{3+} Zeeman levels which operate faster for forbidden ($\Delta m_S = \pm 2$) transitions than for allowed transitions. Using the appropriate rate equations describing the two spin systems and taking into account strong forbidden spin–lattice relaxations, the measured ODEPR effects were explained.

1. Introduction

InP as a compound semiconductor is currently of interest for integrated optical devices. It is grown by the liquid encapsulated Czochralski (LEC) method or by the horizontal Bridgman (LHB) method. As-grown InP crystals are n-type due to shallow donors, but the origin of these shallow donors is not known. A relation with silicon or intrinsic defects is suggested (Cockayne *et al* 1980). For the production of semi-insulating (SI) material InP is doped with iron which acts as a deep acceptor in the Fe^{3+} charge state. Fe^{3+} ($S = \frac{5}{2}$) in InP was investigated with electron paramagnetic resonance (EPR) by Koschel *et al* (1977), Stauss *et al* (1977) and Ippolitova *et al* (1977). Optically detected EPR (ODEPR) spectra were reported by Agool *et al* (1989) and Görger and Spaeth (1991) using an absorption technique (see section 2). In ODEPR the same g factor and five fine-structure split lines were found as in conventional EPR. However, an anomalous change of sign was observed for some of the ODEPR transitions which remains as yet unexplained. The highest and lowest field fine-structure transitions have opposite sign compared to the others. Such behaviour was, for example, not found for the analogous ODEPR spectra of Fe^{3+} in GaAs (Görger and Spaeth 1991).

A similar observation was made when studying the fine-structure split ODEPR lines of Eu^{2+} ($S = \frac{7}{2}$) in BaFBr (Koschnick *et al* 1991). Eu-doped BaFBr is an important x-ray storage phosphor material and recent investigations have been aimed at a better

0953-8984/93/060733+14$07.50

understanding of the defect reactions occurring during storage and read-out processes (Amemiya and Miyahara 1988, Kotera *et al* 1980, Luckey 1975).

In conventional EPR no anomalous intensity changes were observed in both cases.

In this paper we show that the sign-changes of some allowed ODEPR transitions in InP:Fe^{3+} and BaFBr:Eu^{2+} have the same origin, an anomalous spin–lattice relaxation, which connects states differing by $\Delta m_S = \pm 2$ faster than those differing by $\Delta m_S = \pm 1$.

It is shown that the effect of anomalous spin–lattice relaxation is observed in ODEPR using the magnetic circular dichroism of the absorption (MCDA) since the MCDA measures the total spin polarization of the ground state. This is not observable in conventional EPR.

2. Experiment

InP single crystals with an Fe^{3+} concentration of about 10^{16} cm^{-3} were grown by the LEC method (Siemens Erlangen). The crystals were mechanically polished with 3 μm Al_2O_3 and afterwards chemically polished.

Single crystals of BaFBr:Eu^{2+} were grown by the Bridgman–Stockbarger method in graphite crucibles coated with pyrolytic graphite. Eu-doping was performed by adding EuF_3 before crystal growth to the components BaF_2 and $BaBr_2$. The nominal doping level of Eu^{2+} was up to 100 ppm in a reducing atmosphere.

ODEPR was measured as a microwave-induced change of the MCDA with a custom built, computer-controlled ODEPR spectrometer working in the K-band (24 GHz) and at 1.5 K (Ahlers *et al* 1983). The MCDA is the differential absorption of right- and left-circularly polarized light along a static magnetic field. Within the approximation of a small crystal field in comparison to the spin–orbit coupling, it is proportional to the spin polarization of the ground state of a paramagnetic Kramers defect. Usually, upon inducing EPR transitions into the ground-state Zeeman levels, the spin polarization is diminished if the EPR is (partially) saturated between any two levels. This is monitored as a decrease of the MCDA (Ahlers *et al* 1983). With ODEPR one measures the behaviour of the total ground-state spin polarization, in contrast to conventional EPR where only the absorption between those two levels of the spin system, which are in resonance with the applied microwave field, is measured. This difference between ODEPR and conventional EPR is important for systems with $S > \frac{1}{2}$ as will be seen below.

We have performed time-resolved ODEPR experiments to determine the spin–lattice relaxation times T_1 of the spin systems Eu^{2+} and Fe^{3+}. During these experiments the EPR resonance condition of one particular EPR transition was fulfilled and the MCDA was monitored. The microwave power which induced the EPR transition was modulated by a microwave switch. The time behaviour of the MCDA signal was measured using a PC with a built-in transient recording board triggered by the microwave switch controller. After turning off the microwaves the decay of the ODEPR effect was recorded, i.e. the time behaviour of the MCDA signal changing from the diminished MCDA, resulting from the EPR transition, to thermal equilibrium.

3. Experimental results

3.1. The Eu^{2+} defect in BaFBr

Nicollin and Bill (1978) investigated the Eu^{2+} defect in BaFBr with conventional EPR. It was found that Eu^{2+} is incorporated by substituting for a Ba^{2+} ion. Eu^{2+} is a Kramers ion with an s-type ground state, an electron spin of $S = \frac{7}{2}$ (Abragam *et al* 1986) and two naturally occurring isotopes ^{151}Eu (47.82% abundance) and ^{153}Eu (52.18% abundance), each with a nuclear spin of $I = \frac{5}{2}$. The spin Hamiltonian describing the Eu^{2+} spin system can be expressed as follows (Nicollin and Bill 1978):

$$H = \mu_B g B_0 \cdot S + B_2^0 O_2^0 + B_4^0 O_4^0 + B_4^4 O_4^4 + B_6^0 O_6^0 + B_6^4 O_6^4 + AI \cdot S \qquad (1)$$

S and I are the electron and nuclear spin operators, μ_B is the Bohr magneton and g is the electronic g factor. O_i^j and B_i^j are the Stevens vector operators and the Stevens parameters, respectively. A is the hyperfine interaction parameter. Table 1 shows the values of the parameters of equation (1) at $T = 1.5$ K after Nicollin and Bill (1978).

Table 1. Interaction parameters for Eu^{2+} in BaFBr at $T = 1.5$ K after Nicollin and Bill (1978).

g	B_2^0(MHz)	B_4^0(MHz)	B_6^0(MHz)	B_4^4(MHz)	B_6^4(MHz)	^{151}A(MHz)
1.9921	211.1	0.45	0.00095	1.42	0.00952	−97

Eu^{2+} has the following two optical transitions: 4f→5d ($4f^7 \rightarrow 4f^6 5d^1$) and 4f→4f ($^8S_{7/2} \rightarrow {}^6P_J$, $J = \frac{3}{2}, \frac{5}{2}, \frac{7}{2}$, and $^8S_{7/2} \rightarrow {}^6I_J$, $J = \frac{7}{2}, \ldots, \frac{17}{2}$). In BaFCl the 4f→5d transitions are centred around 4.6 eV, and the $^8S_{7/2} \rightarrow 6P_J$, ^6I_J transitions are centred around 3.5 and 3.9 eV, respectively (Brixner *et al* 1980).

In figure 1(*a*) the absorption spectrum and 1(*b*) the MCDA at $T = 1.5$ K are shown for a BaFBr crystal containing 100 ppm Eu^{2+}, as doped in the melt. The dominating MCDA band at 4.5 eV is associated with the 4f→5d transition of Eu^{2+}. The weak partially resolved transitions between 3.8 and 4.0 eV are 4f → 4f transitions. These are nearly unaffected by the difference in the crystal fields of BaFCl and BaFBr (Brixner *et al* 1980).

The MCDA of figure 1(*b*) is, as expected for a paramagnetic system, temperature and magnetic field dependent. It can be quantitively described using a Brillouin function with $S = \frac{7}{2}$ and $g = 1.992$ for Eu^{2+} (Nicollin and Bill 1978). This indicates that in the case of Eu^{2+} in BaFBr the MCDA is proportional to the ground-state spin polarization. This can be explained by the following arguments. The fine-structure splitting of Eu^{2+} (see table 1) is fairly small in comparison to the Zeeman energy because the f electrons of Eu^{2+} are shielded from the crystal field. In the following, we also assume that in the excited 4f or 5d state of the Eu^{2+}, the crystal field is small with respect to the spin–orbit coupling. With this assumption we can use the model of the free ion to calculate the relationship between the MCDA and the populations of the Zeeman levels of the ground state. Then, with the help of the Wigner–Eckart theorem (Messiah 1976) it can be shown that the MCDA is proportional to the ground-state spin polarization.

ODEPR could be measured in the 4f → 5d and 4f → 4f transitions. Figure 2(*a*), curve 2, shows the ODEPR spectrum of a crystal doped with 100 ppm Eu^{2+} measured

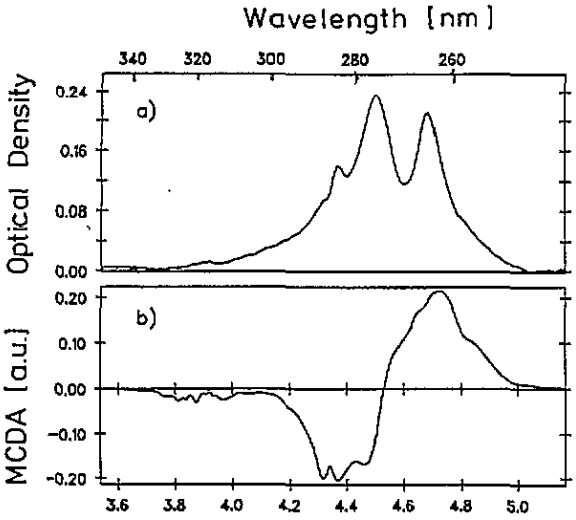

Figure 1. Optical absorption spectrum and MCDA spectrum of the Eu^{2+} defect in BaFBr measured at 1.5 K and a magnetic field of 3 T parallel to the tetragonal c axis.

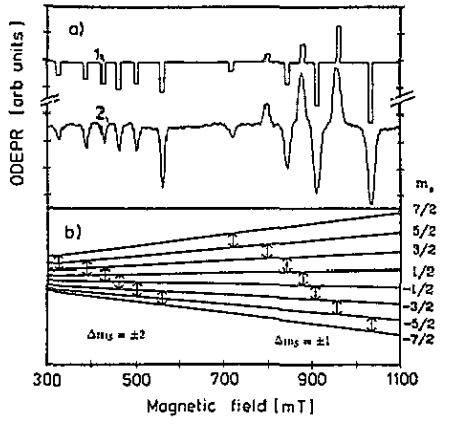

Figure 2. (*a*) Experimental ODEPR spectrum of Eu^{2+} in BaFBr at 1.5 K, 24 GHz and $B \parallel c$-axis measured at 4.37 eV (curve 2). Calculated ODEPR spectrum after determining the rate equations (curve 1). A rectangular ODEPR line shape was assumed in order to simplify the calculations. The experimental line shape is determined essentially by the hyperfine interaction. (*b*) Energy levels and EPR transitions $\Delta m_S = \pm 1$ and $\Delta m_S = \pm 2$. The energy levels were calculated with the spin Hamiltonian parameters after Nicollin and Bill (1978).

at 4.35 eV and 1.5 K. The change of MCDA induced by the microwave transitions is shown as a function of the magnetic field. The expected seven fine-structure lines are measured in the high-field region (Nicollin and Bill 1978). Forbidden transitions with $\Delta m_S = \pm 2$ are seen in the range between 300 mT and 600 mT, and at even lower fields additional transitions assigned to higher values of Δm_S can be observed. The intensity of the forbidden transitions depends very much on the microwave power. All ODEPR line positions, including the forbidden ODEPR transitions below $B = 600$ mT, are explained accurately with the Hamiltonian equation (1) and the interaction parameters of table 1 (see figure 2(*b*) for the energy levels and EPR transitions). Some of the allowed ODEPR transitions ($\Delta m_S = \pm 1$) show a remarkable change of sign. This phenomenon is not influenced by the light intensity, i.e. it is not due to optical pumping effects (Geschwind 1972). Therefore, it arises from an anomalous ODEPR effect which intensifies the MCDA signal and thus intensifies the ground-state polarization. None of the forbidden transitions ($\Delta m_S = \pm 2$) shows such a polarization enhancement.

To investigate the anomalous behaviour of the Eu^{2+} ODEPR, we measured the spin–lattice relaxation time (T_1) of the various ODEPR transitions. At $T = 1.5$ K,

relaxation times of $T_{1,a} \approx 0.3$ s for the allowed and $T_{1,f} \approx 0.06$ s for the forbidden transitions were measured ($T_{1,a}$ stands for T_1 of the allowed and $T_{1,f}$ for T_1 of the forbidden transitions). Figure 3 shows the decay behaviour of an allowed polarization enhancing transition (at 960 mT) and of a forbidden transition (at 560 mT). It is observed that after switching off the microwaves the MCDA of the polarization-enhancing ODEPR transition increases with a time constant of approximatly $T_{1,f}$ and then decays with $T_{1,a}$. The MCDA of those transitions which do not enhance the polarization decay normally with $T_{1,a}$.

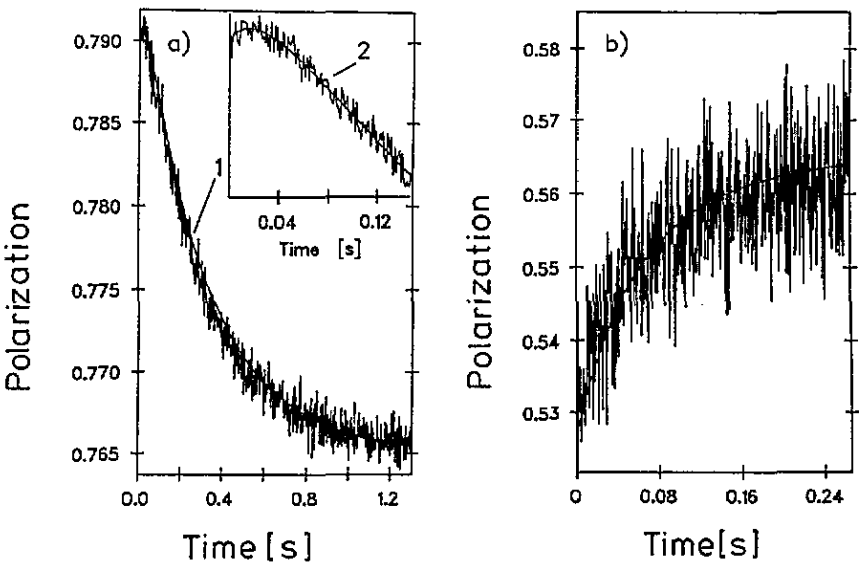

Figure 3. Decay curves of the ODEPR spectrum at $T = 1.5$ K and 4.37 eV. (*a*) Polarization-enhancing ODEPR transition at $B = 960$ mT. The signal increases briefly after switching off the microwaves, as shown in the inset, and then decreases. (*b*) Forbidden ODEPR transition, $B = 560$ mT. In contrast to figure 3(*a*) the ODEPR effect shows 'normal' behaviour, i.e. it reduces the MCDA. After switching off the microwave the MCDA signal increases to its level in thermal equilibrium. The solid lines in (*a*) and (*b*) are the time curves calculated with equation (3) after fitting the parameters ω, ω' and P/P'.

3.2. *The Fe^{3+} defect in InP*

Located on an In site, Fe^{3+} is the neutral charge state with a $3d^5$ configuration and a spin of $\frac{5}{2}$. Upon accepting an electron from a shallow donor or the conduction band, the charge state changes to the diamagnetic Fe^{2+} state. The conventional EPR spectrum of Fe^{3+} is described by the following spin Hamiltonian (Koschel *et al* 1977):

$$H = g\mu_B \boldsymbol{B} \cdot \boldsymbol{S} + (a/6)(S_x^4 + S_y^4 + S_z^4 - (707/16)) \qquad (2)$$

with $g = 2.024$ and $a = 663$ MHz, the cubic splitting parameter.

Agool *et al* (1989) measured the ODEPR spectrum of the Fe^{3+} defect. They observed MCDA enhancing ODEPR transitions and qualitatively explained those with the optical selection rules for the spin-forbidden inner-atomic transition $^6A_1 \rightarrow {}^4T_1$. The situation of the Fe^{3+} defect in InP is similar to that of the Eu^{2+} in BaFBr.

Because of the cubic crystal field, the fine-structure splitting is relatively small in comparison to the Zeeman energy and to the spin–orbit coupling in the excited state. Thus, we can apply the same model of a free ion to calculate the ODEPR effect of the Fe^{3+} ion as in the case of Eu^{2+}. Therefore, the MCDA is proportional to the ground-state spin polarization, as in the case for Eu^{2+} in BaFBr. Our assumption is justified by the experiment where we measured the magnetic field and temperature dependence of the MCDA. This model describes the measured ODEPR properly. We will show in this paper that the optical selection rules have no influence on the ODEPR effect but only on the intensity of the MCDA. The ODEPR effect only depends on the ground-state spin polarization. Furthermore Görger and Spaeth (1991) showed that the optical transitions observed by Agool *et al* (1989) are not inner atomic, but photoionization transitions.

There are two hole-emission charge transfer transitions from Fe^{3+} to Fe^{2+} (Takanohashi and Nakajima 1989, Görger and Spaeth 1991):

$$Fe^{3+} + 0.8\ eV \rightarrow Fe^{2+}(^5E) + h_{VB} \qquad Fe^{3+} + 1.15\ eV \rightarrow Fe^{2+}(^5T_2) + h_{VB}.$$

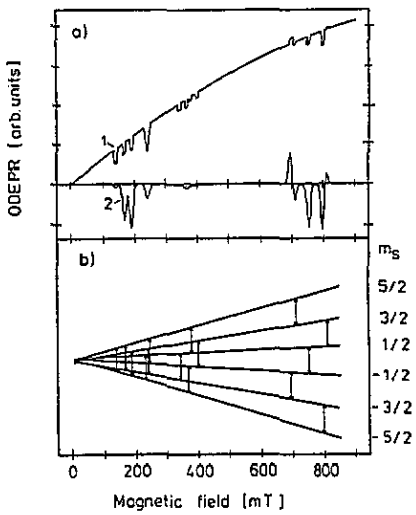

Figure 4. (*a*) Experimental ODEPR spectrum of Fe^{3+} in InP at 1.5 K, 24 GHz and $\boldsymbol{B}$ ||[100] measured at 1.26 eV (curve 2). Calculated MCDA and ODEPR effect after determining the rate equations (curve 1). A simplified line shape (rectangular) was assumed. (*b*) Energy levels and EPR transitions $\Delta m_S = \pm 1, \pm 2, \ldots$. The energy levels are calculated using the spin Hamiltonian parameters determined by Koschel *et al* (1977).

In figure 4(*a*), curve 2, the ODEPR spectrum of Fe^{3+} in InP is shown measured at 1.26 eV in the photoionization transition to the $^5T_2$ state of Fe^{2+}, in figure 4(*b*) the corresponding energy level diagram, calculated with equation (2) (using $g = 2.024$ and $a = 663$ MHz after Koshel *et al* (1977)) is shown with the allowed ($\Delta m_S = \pm 1$) and forbidden ($\Delta m_S = \pm 2, \pm 3, \ldots$) ODEPR transitions. The behaviour of the Fe^{3+} spin system is similar to that of the Eu^{2+} spin system. Some of the allowed ODEPR transitions show a MCDA enhancing effect while all of the forbidden ODEPR lines are MCDA decreasing. The dynamical behaviour of the Fe^{3+} spin system is also similar to that of the Eu^{2+} spin system. Figure 5(*a*) shows the decay of a spin polarization decreasing ODEPR transition ($m_S = \frac{1}{2} \leftrightarrow m_S = -\frac{1}{2}$) and figure 5(*b*) that of a polarization increasing transition ($m_S = -\frac{1}{2} \leftrightarrow m_S = -\frac{3}{2}$). Here also we observe a faster decay of the forbidden ODEPR transtions ($T_{1,f} \approx 0.9$ ms) than of the allowed transitions ($T_{1,a} \approx 2.6$ ms).

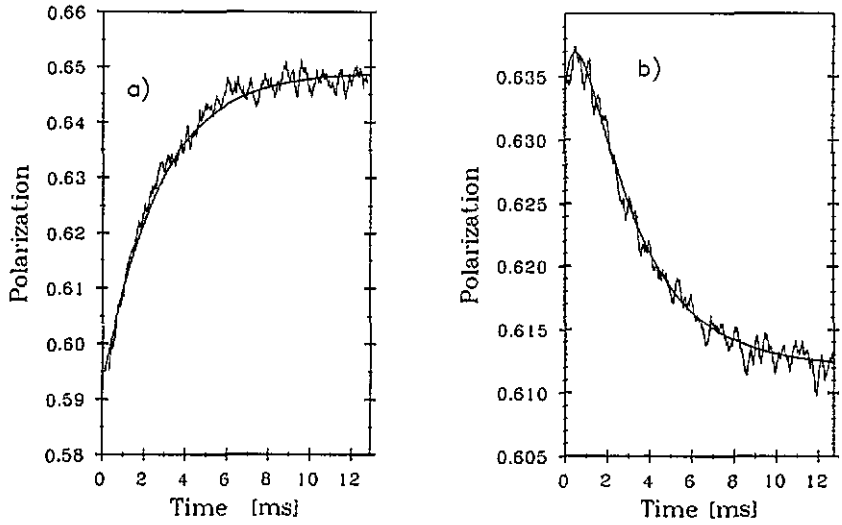

Figure 5. Decay curves of the ODEPR spectrum of Fe^{3+} in InP at $T = 1.5$ K and 1.26 eV, $B \parallel [100]$. (*a*) Polarization decreasing EPR transition $m_S = \frac{1}{2} \leftrightarrow m_S = -\frac{1}{2}$, (*b*) polarization enhancing EPR transition $m_S = -\frac{1}{2} \leftrightarrow m_S = -\frac{3}{2}$. The solid lines are calculated after fitting the parameters ω, ω' and P/P'.

4. Analysis of the dynamical behaviour of the two spin systems

From the T_1 measurements of the forbidden and allowed ODEPR transitions we can see that relaxation after exciting a forbidden transition operates much faster than relaxation after exciting an allowed transition. Presumably the spin system reaches thermal equilibrium with a smaller relaxation rate relaxing over states separated by $\Delta m_S = \pm 1$ compared to states separated by $\Delta m_S = \pm 2$. Proceeding from this observation we developed a model which quantitatively describes these anomalous ODEPR effects. The model is explained for the Eu^{2+} spin system in detail. The Fe^{3+} system can be treated in an analogous way and therefore only the results are presented.

The static and dynamic behaviour of the Eu^{2+} spin system and, thus, the ground-state polarization of the Eu^{2+} ion, can be described by a system of rate equations which consists of a linear differential equation system of first-order with eight linked equations. The transition rates between the levels and thus between the individual equations, are characterized by the spin–lattice relaxations and the EPR transitions. The rate equation system is

$$\mathrm{d}N/\mathrm{d}t = \mathbf{M} \cdot N \tag{3}$$

where

$$N = \begin{pmatrix} n_1 \\ \cdot \\ \cdot \\ \cdot \\ n_8 \end{pmatrix}. \tag{4}$$

$n_1 \ldots n_8$ are the occupancies of the eight Zeeman levels $m_S = -\frac{7}{2}$ to $m_S = \frac{7}{2}$. M is an (8×8) matrix containing all the spin–lattice relaxations and EPR transitions. In table 2 the matrix is listed, where the symbols have the following meanings: P_{ij} = probability of an EPR transition from level i to level j, w_{ij} = relaxation probabilities for the relaxation $i \rightarrow j$.

The next equation holds for the EPR transition probabilities:

$$P_{ij} = P_{ji} \tag{5}$$

$P_{i,i+1}$ is an allowed EPR transition and $P_{i,i+2}$ is a forbidden EPR transition. The spin–lattice relaxation rates obey the following equation (Pake and Estle 1973):

$$w_{i,j}/w_{j,i} = \exp\left(-\Delta E_{i,j}/kT\right) \tag{6}$$

$\Delta E_{i,j}$ is the energy difference between the levels i and j coupled by the spin–lattice relaxation. The requirement (6) follows from the fact that without EPR transitions the spin system tends to go into thermal equilibrium. Only relaxations with $\Delta m_S = \pm 1$ and $\Delta m_S = \pm 2$ were taken into account for the rate equation system. Since the total occupancy remains constant, we can equate $n = \sum_{i=1}^{8} n_i = 1$, which reduces the rate equation system by one equation. The parameters of the differential equation system are the spin–lattice relaxation probabilities $w_{i,i+1}$, $w_{i,i+2}$ and the EPR transition probabilities $P_{i,i+1}$, $P_{i,i+2}$. In order to reduce the total number of parameters, the following assumption was made:

$$\begin{aligned} &\forall i \in \{1 \ldots 7\} \qquad w_{i,i+1} = w \qquad P_{i,i+1} = a_i P \\ &\forall i \in \{1 \ldots 6\} \qquad w_{i,i+2} = w' \qquad P_{i,i+2} = P' \end{aligned} \tag{7}$$

$a_i = |\langle m_{i+i}|S_+|m_i\rangle|^2$ is the relative EPR transition probability between the spin states m_i, m_{i+1} (Abragam and Bleaney 1986). These probabilities can be easily calculated (Abragam and Bleaney 1986) and are shown in table 3 for a spin $\frac{7}{2}$ system (Eu^{2+}) and for a spin $\frac{5}{2}$ system (Fe^{3+}). P is a constant which depends on the microwave power and which is equal for all allowed EPR transitions. The relative probabilities for the forbidden EPR transitions $P_{i,i+2}$ are difficult to estimate. There are several contributions which lead to forbidden transitions: the hyperfine interaction of the electron spin with the nuclear spin, higher-order terms of the fine-structure splitting and off-diagonal elements in the Hamiltonian, produced by a deviation of the magnetic field direction from the orientation of the tetragonal axis of the defect (Abragam and Bleaney 1986). Because of these complications we do not calculate the relative transition probabilities for the forbidden transitions, but we assumed *for simplicity that all forbidden* $\Delta m_S = \pm 2$ *transitions have the same probability* P'. Thus, there remain four parameters. Only the two parameters w and w' are characteristic of the Eu^{2+} spin system. The absolute values of P and P' depend on the microwave power and can be chosen in the experiment. Therefore, only the ratio P/P' enters in the analysis. To measure ODMR, the investigated spin system has to be saturated by microwave transitions. Otherwise, no substantial difference in the populations of the Zeeman levels of the ground state with respect to thermal equilibrium and therefore no difference in the MCDA can be achieved. Therefore, as our calculations have shown, the differences in the probabilities of the various allowed EPR transitions do not critically enter in the results. All transitions fulfil the condition of saturation. Therefore, our approximation of equal probabilities for the forbidden

Table 2. Elements M_{ij} of the spin–lattice relaxation matrix of the Eu^{2+} spin system with $S = \frac{7}{2}$. P_{kl} is the EPR transition probability of the transition $k \rightarrow l$, w_{kl} is the spin–lattice relaxation probability of the relaxation $k \rightarrow l$. (For details see text.)

M_{ij}	1	2	3	4	5	6	7	8
1	$-w_{12} - P_{12}$ $-w_{13} - P_{13}$	$w_{21} + P_{21}$	$w_{31} + P_{31}$	0	0	0	0	0
2	$w_{12} + P_{12}$	$-w_{23} - w_{21}$ $-P_{21} - P_{23}$ $-w_{24} - P_{24}$	$w_{32} + P_{32}$	$w_{42} + P_{42}$	0	0	0	0
3	$w_{13} + P_{13}$	$w_{23} + P_{23}$	$-w_{34} - w_{32}$ $-P_{32} - P_{34}$ $-w_{31} - w_{35}$ $-P_{31} - P_{35}$	$w_{43} + P_{43}$	$w_{53} + P_{53}$	0	0	0
4	0	$w_{24} + P_{24}$	$w_{34} + P_{34}$	$-w_{45} - w_{43}$ $-P_{43} - P_{45}$ $-w_{42} - w_{46}$ $-P_{42} - P_{46}$	$w_{54} + P_{54}$	$w_{64} + P_{64}$	0	0
5	0	0	$w_{35} + P_{35}$	$w_{45} + P_{45}$	$-w_{56} - w_{54}$ $-P_{54} - P_{56}$ $-w_{53} - w_{57}$ $-P_{53} - P_{57}$	$w_{65} + P_{65}$	$w_{75} + P_{75}$	0
6	0	0	0	$w_{46} + P_{46}$	$w_{56} + P_{56}$	$-w_{67} - w_{65}$ $-P_{65} - P_{67}$ $-w_{64} - w_{68}$ $-P_{64} - P_{68}$	$w_{76} + P_{76}$	$w_{86} + P_{86}$
7	0	0	0	0	$w_{57} + P_{57}$	$w_{67} + P_{67}$	$-w_{78} - w_{76}$ $-P_{76} - P_{78}$ $-w_{75} - P_{75}$	$w_{87} + P_{87}$
8	0	0	0	0	0	$w_{68} + P_{68}$	$w_{78} + P_{78}$	$-w_{87} - P_{87}$ $-w_{86} - P_{86}$

Table 3. Relative $\Delta m_s \pm 1$ EPR transition probabilities for a $\frac{7}{2}$ spin system (Eu^{2+}) and a $\frac{5}{2}$ spin system (Fe^{3+}).

	$-\frac{7}{2} \rightarrow -\frac{5}{2}$	$-\frac{5}{2} \rightarrow -\frac{3}{2}$	$-\frac{3}{2} \rightarrow -\frac{1}{2}$	$-\frac{1}{2} \rightarrow +\frac{1}{2}$	$+\frac{1}{2} \rightarrow +\frac{3}{2}$	$+\frac{3}{2} \rightarrow +\frac{5}{2}$	$+\frac{5}{2} \rightarrow +\frac{7}{2}$
Eu^{2+}	7	12	15	16	15	12	7
Fe^{3+}	—	5	8	9	8	5	—

transitions, which are also saturated, is justified. Because of these saturation effects, the ratio P/P' is not unequivocal. Several values of P/P' reproduce the spectra.

For the solution of the equation system (3), a stationary solution was obtained first, i.e. the time derivation of the occupancy vector was set to zero. The hyperfine interaction between the electronic spin and the spin of the central nucleus was not taken into account. Only w/w' is determined from this solution. Subsequently the dynamical solution, which describes the time behaviour of the ODEPR transition after switching off the microwave power, was determined numerically at the resonant conditions of the ODEPR transition. This dynamical behaviour is described by the ground-state spin polarization

$$P(t) = \frac{1}{S}\sum_{i=1}^{8} n_i(t)m_i$$

(the m_i are the magnetic quantum numbers m_S of the Zeeman levels of the spin system).

The three parameters $(w, w', P/P')$ were determined by fitting the dynamical solution to the measured T_1 times and by fitting the steady-state solution to the measured ODEPR spectrum. The results of the calculation can be seen in figures 2(*a*) and 3 for the ODEPR spectrum (stationary solution) and the time behaviour of the ODEPR transition (dynamical solution). In table 4 the parameters obtained for the spin–lattice relaxation probabilities and the ratio P/P' of the ODEPR transition probabilities are given for $T = 1.5$ K. We must stress again that the ratio P/P' is not unequivocal. It may vary in a relatively wide range because of saturation effects as pointed out previously. In spite of this, we include P/P' in table 4 to show all parameters with which we performed the calculations. The dynamical solution of the ground-state spin polarization is a linear combination of seven exponential functions and the constant steady-state solution. Therefore, we obtain seven different time constants describing the polarization changes at the beginning of an ODEPR transition or immediately thereafter:

$$N(t) = \sum_{i=1}^{7} C_i V_i e^{\lambda_i t} + N_{\text{stat}}. \tag{8}$$

λ_i are the eigenvalues of the relaxation matrix and V_i are the eigenvectors. N_{stat} is the stationary population of the Zeeman levels of the spin system. The sum in (8) describes the dynamical behaviour of the population of the Zeeman levels, for example, after switching off the microwaves. The MCDA is proportional to the ground-state spin polarization:

$$\text{MCDA} \propto P(t) = \frac{1}{S}\sum_{i=1}^{8} n_i(t)m_i = \frac{1}{S}\left[\sum_{j=1}^{7} \underbrace{C_j \sum_{i=1}^{8} m_i V_{j,i}}_{K_j} e^{\lambda_j t} + \sum_{i=1}^{8} m_i n_{i_{\text{stat}}}\right]. \tag{9}$$

For the time constants of the exponentials one obtains

$$T_j = -1/\lambda_j. \tag{10}$$

We get the ground-state spin-polarization and the MCDA:

$$\text{MCDA} \propto P(t) = \frac{1}{S}\left[\sum_{j=1}^{7} K_j e^{-t/T_j} + \sum_{i=1}^{8} m_i n_{i_{\text{stat}}}\right]. \tag{11}$$

In table 5 the time constants and the accompanying expansion coefficients K_j of the exponential functions are given for the time behaviour of an allowed and a forbidden ODEPR transition. They are calculated by fitting to the experimental data. Infinity (∞) represents the steady-state solution which is the MCDA effect without any microwave irradiation and has the time constant with the largest coefficient K_i. It can be seen that in addition to the steady-state solution only the largest time constant has a significant effect on the time behaviour of the ODEPR effect. This time is of course in good agreement with the measured times $T_{1,a} = 0.3$ s and $T_{1,f} = 0.06$ s because of the fitting. In table 5 these values are printed in bold.

Table 4. Parameters of the rate equation system (3) for Eu^{2+} in BaFBr.

$w(s^{-1})$	$w'(s^{-1})$	P/P'
0.7	10	4

Table 5. Time constants and expansion coefficients describing the decay of the ODEPR effect of the allowed transition P_{23} (see figure 3) at $B = 960$ mT and the forbidden transition P_{13} at $B = 560$ mT within the Eu^{2+} spin system at $T = 1.5$ K.

P_{23}, $B = 960$ mT		P_{13}, $B = 560$ mT	
Time constant T_i (s^{-1})	Coefficient K_i	Time constant T_i (s^{-1})	Coefficient K_i
∞	-7.65×10^{-1}	∞	-5.67×10^{-1}
0.3168	-2.94×10^{-2}	0.3515	3.01×10^{-3}
0.0301	3.60×10^{-3}	**0.0663**	1.73×10^{-2}
0.0262	8.52×10^{-5}	0.0553	-1.32×10^{-3}
0.0152	8.41×10^{-4}	0.0266	2.21×10^{-3}
0.0140	2.06×10^{-5}	0.0247	-2.54×10^{-4}
0.0106	8.50×10^{-5}	0.0164	3.54×10^{-4}
0.0093	4.43×10^{-6}	0.0155	-1.73×10^{-5}

The ODEPR transition probabilities P and P' were of course dependent on the selected microwave power in the experiment. Simulations of the ODEPR effect have shown that the polarization enhancing effect occurs only when the following condition holds:

$$w' > 6w. \tag{12}$$

This confirms the assumption that strong spin–lattice relaxation across the $\Delta m_S = \pm 2$ transition causes the unusual ODEPR effect in the Eu^{2+} spin system in BaFBr.

With the model presented here a qualitative description of a polarization enhancing transition would be as follows (taking the transition $2 \rightarrow 3$ at $B = 960$ mT

as an example, figure 6): While transferring spin occupancy from level 2 to level 3 via resonant microwave irradiation a strong $\Delta m_S = \pm 2$ relaxation $3 \rightarrow 1$ takes place. This means that the spin occupancy of level 2 is not transferred to level 3 but to level 1 and thus the polarization of the spin system is increased although the ODEPR transition transfers spins to a higher level. The alternating signs of the allowed ODEPR transitions (some allowed transitions are not polarization enhancing, see figure 2(*a*)) are the result of the complex polarization behaviour of the complete spin system which is calculated by summation over the occupancy of all spin states.

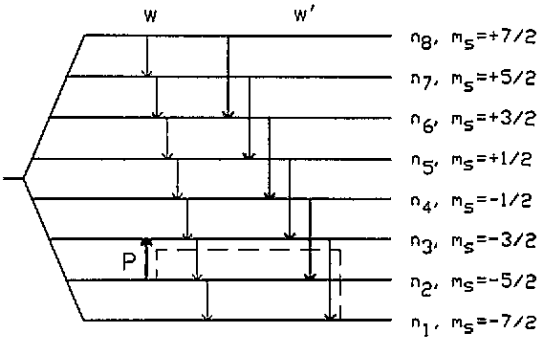

Figure 6. Spin–lattice relaxation model of the Eu^{2+} spin system in BaFBr. The energy levels are only drawn schematically. See text for explanation.

However, with a simple approximation this behaviour can also be understood qualitatively. If the condition $w' \gg w$ holds, we can neglect w. Then, we can consider two independent spin reservoirs. The first spin reservoir (R1) consists of the levels: 1,3,5,7 ($m_S = -\frac{7}{2}, -\frac{3}{2}, \frac{1}{2}, \frac{5}{2}$) and the second one (R2) consists of the levels: 2,4,6,8 ($m_S = -\frac{5}{2}, -\frac{1}{2}, \frac{3}{2}, \frac{7}{2}$) (see figure 6). The contribution of R1 to the total spin polarization is larger than that of R2. Without microwave transitions, a Boltzman equilibrium is achieved inside each reservoir. Both reservoirs are connected via allowed EPR transitions. Exciting a transition from the second reservoir (R2) to the first (R1) increases the population of R1 at the expense of R2 thus increasing the polarization. On the other hand, exciting a transition from R1 to R2 has the opposite effect and the polarization is decreased. The alternating signs of the ODEPR transitions are caused by alternately exciting a transition from R1 to R2 and from R2 to R1.

A forbidden ($\Delta m_S = \pm 2$) transition cannot have any polarization enhancing properties within our model because of the restriction $\Delta m_S \leqslant \pm 2$. Higher relaxations than those across $\Delta m_S = \pm 2$ seem to play no role in describing the Eu^{2+} spin system in BaFBr, because the measured ODEPR effects could be explained excellently only by the two relaxations $\Delta m_S = \pm 1, \pm 2$. A similiar behaviour of the spin system was found for Eu^{2+} in SrFBr.

If an analogous mathematical procedure is used for the Fe^{3+} defect in InP the behaviour of the Fe^{3+} spin system can also be described. The results of the calculations for the polarization enhancing ODEPR effect and the relaxation behaviour of the Fe^{3+} spin system are shown in figure 4(*a*), curve 1 and figure 5. Since the total spin of Fe^{3+} is $\frac{5}{2}$, the relaxation matrix has the dimension six and, therefore, equation (3) consists of six linked equations instead of eight. In table 6 the elements of this matrix are presented. Fitting the Fe^{3+} rate equations to the ODEPR spectrum

yields the parameters of table 7 which can be interpreted in a similar way as the parameters of table 4 for Eu^{2+}. The time constants and expansion coefficients for an allowed polarization enhancing and an allowed polarization decreasing transition are shown in table 8. It is seen that there is also good agreement between the measured and calculated curves (figure 5).

Table 6. Elements M_{ij} of the spin–lattice relaxation matrix of the Fe^{3+} spin system with S = 5/2. The meaning of the symbols are the same as in table 2.

M_{ij}	1	2	3	4	5	6
1	$-\omega_{12}-P_{12}$ $-\omega_{13}-P_{13}$	$\omega_{21}+P_{21}$	$\omega_{31}+P_{31}$	0	0	0
2	$\omega_{12}+P_{12}$	$-\omega_{21}-P_{21}$ $-\omega_{23}-P_{23}$	$\omega_{32}+P_{32}$	$\omega_{42}+P_{42}$	0	0
3	$\omega_{13}+P_{13}$	$\omega_{23}+P_{23}$	$-\omega_{31}-P_{31}$ $-\omega_{32}-P_{32}$ $-\omega_{34}-P_{34}$ $-\omega_{35}-P_{35}$	$\omega_{43}+P_{43}$	$\omega_{53}+P_{53}$	0
4	0	$\omega_{24}+P_{24}$	$\omega_{34}+P_{34}$	$-\omega_{42}-P_{42}$ $-\omega_{43}-P_{43}$ $-\omega_{45}-P_{45}$ $-\omega_{46}-P_{46}$	$\omega_{54}+P_{54}$	$\omega_{64}+P_{64}$
5	0	0	$\omega_{35}+P_{35}$	$\omega_{45}+P_{45}$	$-\omega_{53}-P_{53}$ $-\omega_{54}-P_{54}$ $-\omega_{56}-P_{56}$	$\omega_{65}+P_{65}$
6	0	0	0	$\omega_{46}+P_{46}$	$\omega_{56}+P_{56}$	$-\omega_{63}-P_{63}$ $-\omega_{64}-P_{64}$ $-\omega_{65}-P_{65}$

Table 7. Parameters of the rate equation system (3) for Fe^{3+} in InP.

$w(s^{-1})$	$w'(s^{-1})$	P/P'
90	450	3

Table 8. Time constants and expansion coefficients for describing the decay of the ODEPR effect of the allowed transitions P_{12} at $B = 805$ mT and the forbidden transition P_{13} at $B = 387$ mT within the Fe^{3+} spin system at $T = 1.5$ K.

$m_S = -\frac{1}{2} \leftrightarrow m_S = -\frac{5}{2}$; B_0 =387 mT		$m_S = -\frac{3}{2} \leftrightarrow m_S = -\frac{5}{2}$; B_0 =805 mT	
Time constant T_i (ms^{-1})	Coefficient K_i	Time constant T_i (ms^{-1})	Coefficient K_i
∞	-3.77×10^{-1}	∞	-6.49×10^{-1}
3.78	-8.47×10^{-3}	**2.60**	$\mathbf{5.65 \times 10^{-2}}$
0.88	$\mathbf{3.726 \times 10^{-2}}$	0.68	-3.57×10^{-3}
0.76	4.52×10^{-4}	0.56	1.09×10^{-3}
0.31	3.39×10^{-3}	0.28	5.91×10^{-5}
0.30	-3.97×10^{-4}	0.28	-1.19×10^{-4}

The effect of the anomalous spin–lattice relaxation was observed for spin systems with $S > \frac{1}{2}$ in quite different materials: an ionic crystal and a typical semiconductor. However, the effect seems not to be characteristic of the paramagnetic ion, but rather of the host lattice. In ODEPR experiments using the same measurement technique

for Fe^{3+} in GaAs, no anomalous sign effects were observed, while only the low field $\Delta m_S = \pm 1$ line of Fe^{3+} in GaP showed a polarization enhancement. The reason for the occurrence of anomalous spin–lattice relaxations is not yet understood. It has to be stressed once again that this effect is only measurable by ODEPR and not by conventional EPR since EPR detects only the transition rate between two adjacent levels whereas ODEPR reveals the total polarization of a spin system.

5. Conclusions

The ODEPR spectrum of certain high-spin systems measured with the MCDA technique may show ground-state polarization enhancement. Two examples were presented here, the Eu^{2+} ion in BaFBr and the Fe^{3+} ion in InP. This anomalous effect can be explained by a forbidden spin–lattice relaxation which operate faster between states differing by $\Delta m_S = \pm 2$ than between those with $\Delta m_S = \pm 1$. The polarization enhancement is in principle not detectable by conventional EPR where only the absorption of the microwave quanta inducing an EPR transition between two adjacent Zeeman levels is seen. For the occurrence of the anomalous spin–lattice relaxation the host crystal plays an important role since for the same paramagnetic ion (Fe^{3+}) in a similar crystal (GaAs) the polarization enhancement is not observed.

References

Abragam A and Bleaney B 1986 *Electron Pramagnetic Resonance of Transition Ions* (New York: Dover)

Agool I R, Deiri M and Cavenett B C 1989 *Semicond. Sci. Technol.* 4 48

Ahlers F J, Lohse F, Spaeth J-M and Mollenauer L F 1983 *Phys. Rev.* B **28** 1249

Amemiya Y and Miyahara J 1988 *Nature* **336** 89

Brixner L H, Bierlein J D, Johnson V 1980 *Eu^{2+} Fluorescence and its Application in Medical X-ray Intensifying Screens (Current Topics in Material Science 4)* (Amsterdam: North-Holland) p 47

Cockayne B, MacEwan W R and Brown G T 1980 *J. Mater. Sci.* **15** 2785

Geschwind S 1972 *Electron Paramagnetic Resonance* (New York: Plenum)

Görger A and Spaeth J-M 1991 *Semicond. Sci. Technol.* **6** 800

Ippolitova G K, Omel'yanowskiĭ É M, Pavlov N M Nashelśkiĭ A Y and Yakobson S V 1977 *Sov. Phys.–Semicond.* **11** 1773

Kittel Ch 1976 *Introduction to Solid State Physics* (New York: Wiley)

Koschel W H, Kaufmann U and Bishop S G 1977 *Solid State Commun.* **21** 1069

Koschnick F K, Spaeth J-M, Eachus R S, McDugle W G and Nuttal R H 1991 *Phys. Rev. Lett.* **67** 3571

Kotera N, Eguchi S, Miyahara J, Matsumoto S and Kato H 1980 *US Patent* 4 239 968

Luckey G W 1975 *US Patent* 3 859 527 Revised 31847 (1983)

Messiah A 1976 *Quantum Mechanics* (New York: Wlley)

Nicollin D and Bill H 1978 *J. Phys. C: Solid State Phys.* **11** 4803

Pake G E and Estle T L 1973 *The Physical Principles of Electron Paramagnetic Resonance* (New York: Addison-Wesley)

Stauss G H, Krebs J J and Henry R C 1977 *Phys. Rev.* B **16** 974

Takanohashi T and Nakajima K 1989 *J. Appl. Phys.* **65** 3933